Structures of diffusion regions in collisionless magnetic reconnection

Takayuki Umeda,[a] Kentaro Togano, and Tatsuki Ogino
Solar-Terrestrial Environment Laboratory, Nagoya University, Nagoya, Aichi 464-8601, Japan

(Received 8 January 2010; accepted 31 March 2010; published online 7 May 2010)

Detailed structures of diffusion regions in two-dimensional collisionless magnetic reconnection are studied by using an electromagnetic Vlasov simulation. It has been well known that plasma number density decreases near the X-point of the reconnection. However, numerical thermal fluctuations exist in particle-in-cell simulations, and there is a possibility that detailed structures near the X-point diffuse numerically when the number of particles per cell is not enough. In the present study, a high-resolution two-dimensional Vlasov simulation is performed. It is found that electron number density in the electron diffusion region decreases to a hundredth of the initial value. Structures of electron diffusion region are determined by the local electron inertial length. © *2010 American Institute of Physics*. [doi:10.1063/1.3403345]

I. INTRODUCTION

Magnetic reconnection is an important process with fast conversion of energy stored in a compressed magnetic field into plasma kinetic energy. The rate of reconnection is controlled by a narrow region around the reconnection point (X-point) called the "diffusion region," where magnetic dissipative effects enable magnetic field lines to reconnect. The Geospace Environment Modeling (GEM) reconnection challenge and related works (e.g., Refs. 1–3) have been shown that reconnection processes are controlled by ion dynamics and that a high reconnection rate results from the Hall effect, i.e., decoupling between ions and electrons. In a kinetic plasma, structures of the diffusion region are thought to consist of an inner electron region and an outer ion region, and spatial scales of the ion and electron diffusion regions are determined by each inertial length.

The recent full particle-in-cell (PIC) simulations, however, have shown that the length of electron current sheet extends in the outflow direction.[4,5] Two-scale structures of electron diffusion region have been reported in more recent large-scale two-dimensional (2D) PIC simulations.[6,7] These simulations indicate that the outer diffusion region is formed by electron outflow jets, with a length tens of ion inertial length. Properties of electron diffusion region are also studied from various physical quantities obtained in PIC simulations.[8,9] Such multiscale structures of electron diffusion region are also studied by means of *in situ* observations in the Earth's magnetosphere (e.g., Refs. 10 and 11).

It has been well known that plasma number density decreases near the X-point of the reconnection. In the PIC model, however, numerical thermal fluctuations are strongly enhanced when the number of particles per cell becomes lower. Thus, there is a possibility that the detailed structures near the X-point diffuse numerically in PIC simulations with a low number of particles per cell. The Vlasov method is considered to be an alternative to the PIC method because the Vlasov method is free from the numerical thermal fluctuations. However, one needs a huge computational resource for a hyperdimensional Vlasov simulation. In recent days, numerical techniques for the Vlasov model are rapidly developing. Very recently, there are several successful simulations of magnetic reconnection via five-dimensional (5D) Vlasov simulations with 2D configuration and three-dimensional (3D) velocity dimensions.[12,13]

In the present study, we study detailed structures of diffusion regions in a symmetric magnetic reconnection via a Vlasov simulation. In typical PIC simulations of 2D magnetic reconnection, the number of particles per cell at the incoming boundary is 100, and therefore the number of particles per cell at the center of the current sheet becomes 500–1000. When the number of particles per cell decreases to a hundredth, it is not easy to support fine structures around diffusion regions by 5–10 particles per cell because of the enhanced thermal fluctuations in the PIC method. We think that the Vlasov method would have a benefit that can treat low-density regions near the X-point of the reconnection without numerical noises.

This paper is structured as follows. Simulation setup for the magnetic reconnection is presented in Sec. II. Numerical results are presented in Sec. III. Summary is given in Sec. IV.

II. SIMULATION METHOD AND MODEL

We use a 5D electromagnetic Vlasov code with 2D configuration and 3D velocity dimensions,[13] in which the full set of Maxwell's equations for electromagnetic fields (1) and the Vlasov equation for collisionless charged particles (2) are solved self-consistently,

$$\left.\begin{aligned} \nabla \times \vec{B} &= \mu_0 \vec{J} + \frac{1}{c^2}\frac{\partial \vec{E}}{\partial t} \\ \nabla \times \vec{E} &= -\frac{\partial \vec{B}}{\partial t} \\ \nabla \cdot \vec{E} &= \frac{\rho}{\epsilon_0} \\ \nabla \cdot \vec{B} &= 0 \end{aligned}\right\}, \tag{1}$$

[a]Electronic mail: umeda@stelab.nagoya-u.ac.jp.

$$\frac{\partial f_s}{\partial t} + \vec{v}\frac{\partial f_s}{\partial \vec{x}} + \frac{q_s}{m_s}(\vec{E} + \vec{v} \times \vec{B})\frac{\partial f_s}{\partial \vec{v}} = 0, \tag{2}$$

where $\vec{E}$, $\vec{B}$, $\vec{J}$, ρ, μ_0, ϵ_0, and c represent electric field, magnetic field, current density, charge density, magnetic permeability, dielectric constant, and light speed, respectively. The distribution functions $f_s(\vec{x},\vec{v},t)$ are defined in a position-velocity phase space. The subscript s represents the singly charged ions and electrons (e.g., $s=i,e$). The quantities q_s and m_s are the charge and mass of particle species s. The current density $\vec{J}$ is determined so that ρ and $\vec{J}$ satisfy the current-continuity equation

$$\frac{\partial \rho}{\partial t} + \nabla \cdot \vec{J} = 0. \tag{3}$$

The electromagnetic fields are discretized on the Yee[14] grid system, and the implicit Finite Difference Time Domain (FDTD) method is adopted to solve Maxwell's equations, which is free from the Courant–Friedrichs–Lewy (CFL) condition for electromagnetic light mode waves. For stable numerical integration of the Vlasov equation (2), we adopt the operator splitting technique (e.g., Refs. 15 and 16). The Vlasov equation splits into the following three equations:

$$\frac{\partial f_s}{\partial t} + \vec{v}\frac{\partial f_s}{\partial \vec{x}} = 0, \tag{4}$$

$$\frac{\partial f_s}{\partial t} + \frac{q_s}{m_s}\vec{E}\frac{\partial f_s}{\partial \vec{v}} = 0, \tag{5}$$

$$\frac{\partial f_s}{\partial t} + \frac{q_s}{m_s}(\vec{v} \times \vec{B})\frac{\partial f_s}{\partial \vec{v}} = 0. \tag{6}$$

Equations (4) and (5) are scalar (linear) advection equations in which $\vec{v}$ and $\vec{E}$ are independent of $\vec{x}$ and $\vec{v}$, respectively. It should be noted that it is essential to satisfy the current-continuity equation. We use a multidimensional conservative scheme for solving the advection equation,[13] in which the charge continuity equation and Poisson's equation are exactly satisfied. Equation (6), on the other hand, is a multidimensional rotation equation which follows a circular motion of a profile at constant speed by a centripetal force. For stable rotation of the profile on the Cartesian grid system, the "back-substitution" technique[17] is applied. We need a numerical interpolation scheme to solve Eqs. (4)–(6). We use a higher-order, positive, nonoscillatory, and conservative semi-Lagrangian scheme[18] which preserves positivity and suppresses unphysical numerical oscillations by using a "nonoscillatory" limiter. The detailed descriptions of the numerical schemes are given in Refs. 13, 17, and 18.

As demonstrated by Umeda *et al.*,[13] a numerical constraint on the spatial grid can be relaxed in the full-electromagnetic Vlasov simulation. That is, the grid spacing can be taken to be much longer than the electron Debye length if the Debye-scale physics can be negligible. It should be noted, however, that low resolutions in configuration or velocity spaces sometimes cause numerical diffusion of physical structures. In the present Vlasov code, there is a numerical constraint on the CFL condition for rotation in velocity space by magnetic fields. For stable rotation of distribution functions with the back-substitution scheme on the Cartesian grid system, we choose the time step Δt such that

$$\Delta v_e > \frac{q_e}{m_e}|\vec{v}_{\max,e}|B_0\Delta t = \omega_{ce}|\vec{v}_{\max,e}|\Delta t. \tag{7}$$

The initial condition is based on a Harris-type sheet equilibrium[19] in the x-y plane,

$$B_x^{t=0}[y] = -B_0 \tanh\left[\frac{y}{\lambda}\right], \tag{8}$$

where λ is the half thickness of the current sheet. Let us assume that the initial electrons and ions have a shifted Maxwellian distribution

$$f_s[\vec{x},\vec{v}] = \frac{n[y]}{(\sqrt{2\pi}V_{ts0})^3}\exp\left[\frac{v_x^2 + v_y^2 + (v_z - V_{ds}[y])^2}{2V_{ts0}^2}\right], \tag{9}$$

and that the initial density distribution is given by

$$n^{t=0}[y] = n_0\left\{\frac{(1-\alpha)}{\cosh^2\left[\frac{y}{\lambda}\right]} + \alpha\right\}. \tag{10}$$

Here the factor α denotes the ratio of the background number density (at $y=\pm\infty$) to the current sheet number density (at $y=0$). Inserting Eqs. (9) and (8) into the Vlasov equation with $\partial/\partial t=0$, we obtain

$$V_{di}^{t=0}[y] = \frac{V_{di0}}{1-\alpha+\alpha\cosh^2\left[\frac{y}{\lambda}\right]}, \quad V_{di0} = \frac{2m_iV_{ti0}}{q_iB_0\lambda} \tag{11}$$

and

$$V_{de}^{t=0}[y] = \frac{V_{de0}}{1-\alpha+\alpha\cosh^2\left[\frac{y}{\lambda}\right]}, \quad V_{de0} = -\frac{2m_eV_{te0}}{q_eB_0\lambda} \tag{12}$$

with

$$n_0 = \frac{B_0}{q\mu_0(V_{di0} - V_{de0})\lambda}. \tag{13}$$

Thus the magnitude of magnetic field at $y=\pm\infty$ is written as

$$B_0 = \frac{\sqrt{2\left(\frac{m_i^2}{q_i^2}\omega_{pi0}^2V_{ti0}^2 + \frac{m_e^2}{q_e^2}\omega_{pe0}^2V_{te0}^2\right)}}{c}. \tag{14}$$

Hence, the present study concerns a symmetric reconnection.

We adopt the one quarter model with the symmetry constraints at $x=0$ and $y=0$. Thus, the simulation domain is taken for $x=0\sim L_x(=12.8d_{i0})$ in the x direction and $y=0\sim L_y(=6.4d_{i0})$ in the y direction, where d_{i0} is the initial ion inertial length ($d_{i0}=c/\omega_{pi0}$) at the center of the current sheet ($y=0$). The sheet half thickness is chosen to be $\lambda=0.5d_{i0}$. To normalize the physical quantities, we choose the initial (constant) electron thermal velocity as $V_{te0}=1$ and the electron plasma frequency at $y=0$ as $\omega_{pe0}=1$. Thus, the electron Debye length at $y=0$ becomes $\lambda_{De0}=V_{te0}/\omega_{pe0}=1$. In order to make a difference between the inertial length and the

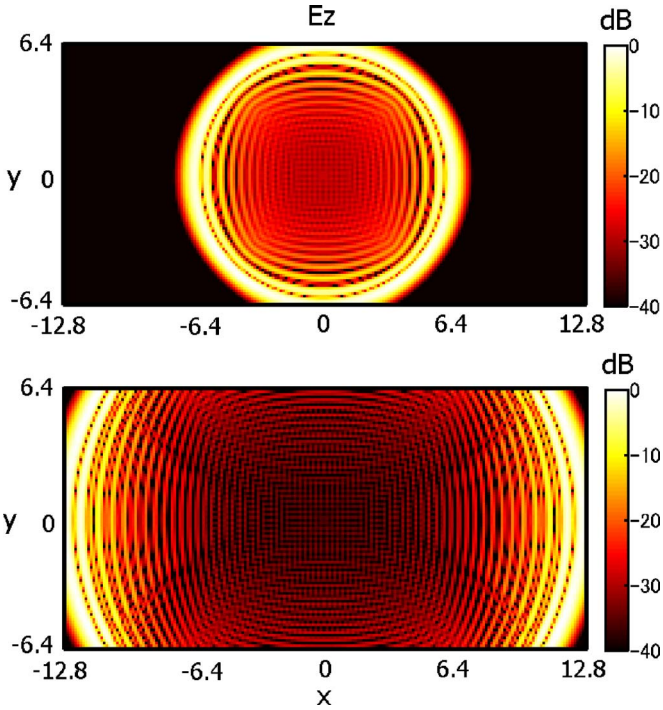

FIG. 1. (Color online) Out-of-plane electric field (reconnection rate: E_z) resulting from an electromagnetic radiation at the center of the simulation domain. (Top) The wave reaches the boundaries in the y direction. (Bottom) The wave reaches the boundaries in the x direction.

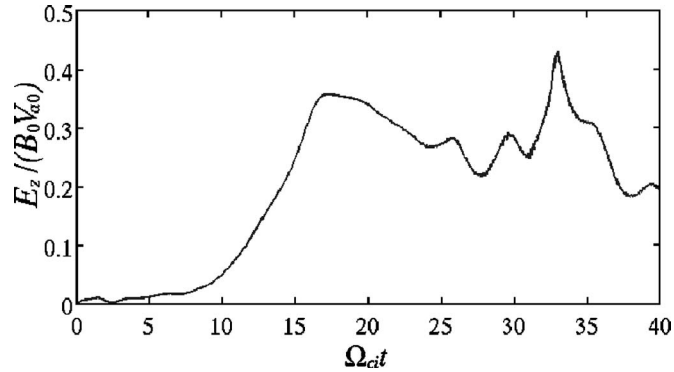

FIG. 2. Out-of-plane electric field (reconnection rate: E_z) at the center of the simulation domain as a function of time. The electric field is normalized by B_0V_{a0}.

Debye length, we choose the light speed and the electron cyclotron frequency as $c/V_{te0}=20.0$ and $\Omega_{ce0}/\omega_{pe0}=0.2$, where Ω_{c0} denotes the cyclotron frequency at $y=\pm\infty$. However, the ion-to-electron mass ratio is reduced to $m_i/m_e=25$ for limitation of our computational resource. The temperature ratio is set as $T_i/T_e=7$. Then, the ratio of light speed to the "effective" Alfvén speed becomes $c/V_{a0}=25$, where $V_{a0}\equiv c\Omega_{ci0}/\omega_{pi0}$. Note that Ω_{ci0} and ω_{pi0} are defined at $y=\pm\infty$ and $y=0$, respectively, in common with the GEM reconnection challenge.[1] The ion and electron inertial lengths become $d_{i0}/\lambda_{De0}=100.0$ and $d_{e0}/\lambda_{De0}=20.0$, respectively. The drift velocities are obtained as $V_{di0}/V_{te0}=1.4$ and $V_{de0}/V_{te0}=-0.2$. The background density ratio is chosen to be $\alpha=0.1$.

We use $N_x\times N_y=320\times 160$ grid points for the configuration space and $N_{vx}\times N_{vy}\times N_{vz}=40\times 40\times 40$ grid points for the velocity space. The grid spacing in the configuration and velocity spaces are $\Delta x=4\lambda_{De0}(=0.04d_{i0})$ and $\Delta v=0.4V_{ts0}$, respectively. The time step is set as $\omega_{pe0}\Delta t=0.1$. A weak perturbation with a long wavelength is employed to initiate reconnection at the center of the simulation domain (e.g., Ref. 1).

At the outer boundary ($x=L_x$ and $y=L_y$), we imposed the open boundary condition where outgoing plasmas and electromagnetic waves are absorbed while incoming plasmas are determined so that a zero normal derivative condition is enforced. In the PIC method, we need to extrapolate velocity distribution functions at boundaries and approximate inward flux of plasma particles from the boundaries by using several sets of uniformly distributed random numbers (e.g., Ref. 5). In the Vlasov method, on the other hand, it is easy to enforce the zero normal derivative condition by inserting values at neighboring cells into boundary cells.

Absorbing boundary conditions for outgoing electromagnetic waves are a difficult problem in numerical simulations. In the present study, we employ a "radiation" boundary condition (e.g., Refs. 5, 20, and 21). The radiation boundary condition is based on the one-dimensional wave equations,

$$\frac{\partial f}{\partial t}\pm c\frac{\partial f}{\partial x}=0 \tag{15}$$

for boundaries in the x direction and

$$\frac{\partial g}{\partial t}\pm c\frac{\partial g}{\partial y}=0 \tag{16}$$

for boundaries in the y direction, where $f\equiv E_z\pm cB_y$ and $E_y\mp cB_z$, and $g\equiv E_z\mp cB_x$ and $E_x\pm cB_z$. To demonstrate that the present boundary conditions are open with respect to electromagnetic radiation, an electromagnetic wave is radiated at the center of the simulation domain. As shown in Fig. 1, a large amplitude radiation front propagates outward at the light speed c at an early time, and the wave leaves the system at a later time. Reflections at the boundaries are quite small (less than -40 dB), and there is no observable accumulation of electromagnetic radiation over longer periods. It should be noted that "resistive" boundary conditions are also used in kinetic plasma simulations (e.g., Refs. 22 and 23). However, these methods require additional grid cells for resistive layers for wave absorption. The resistive boundary conditions are computationally expensive in Vlasov simulations.

III. SIMULATION RESULTS

As a measure of the reconnection rate, we plot the time evolution of the out-of-plane electric field (E_z) at the center of the simulation domain (X-point) in Fig. 2. The reconnection rate develops in association with the evolution of magnetic reconnection, and the "fast reconnection" ($E_z>0.1B_0V_{a0}$) is achieved for $\Omega_{ci0}t>12$. The reconnection saturates at $\Omega_{ci0}t\sim 17$ with the reconnection rate of $E_z\sim 0.35B_0V_{a0}$, and then decreases to a quasi-steady-state

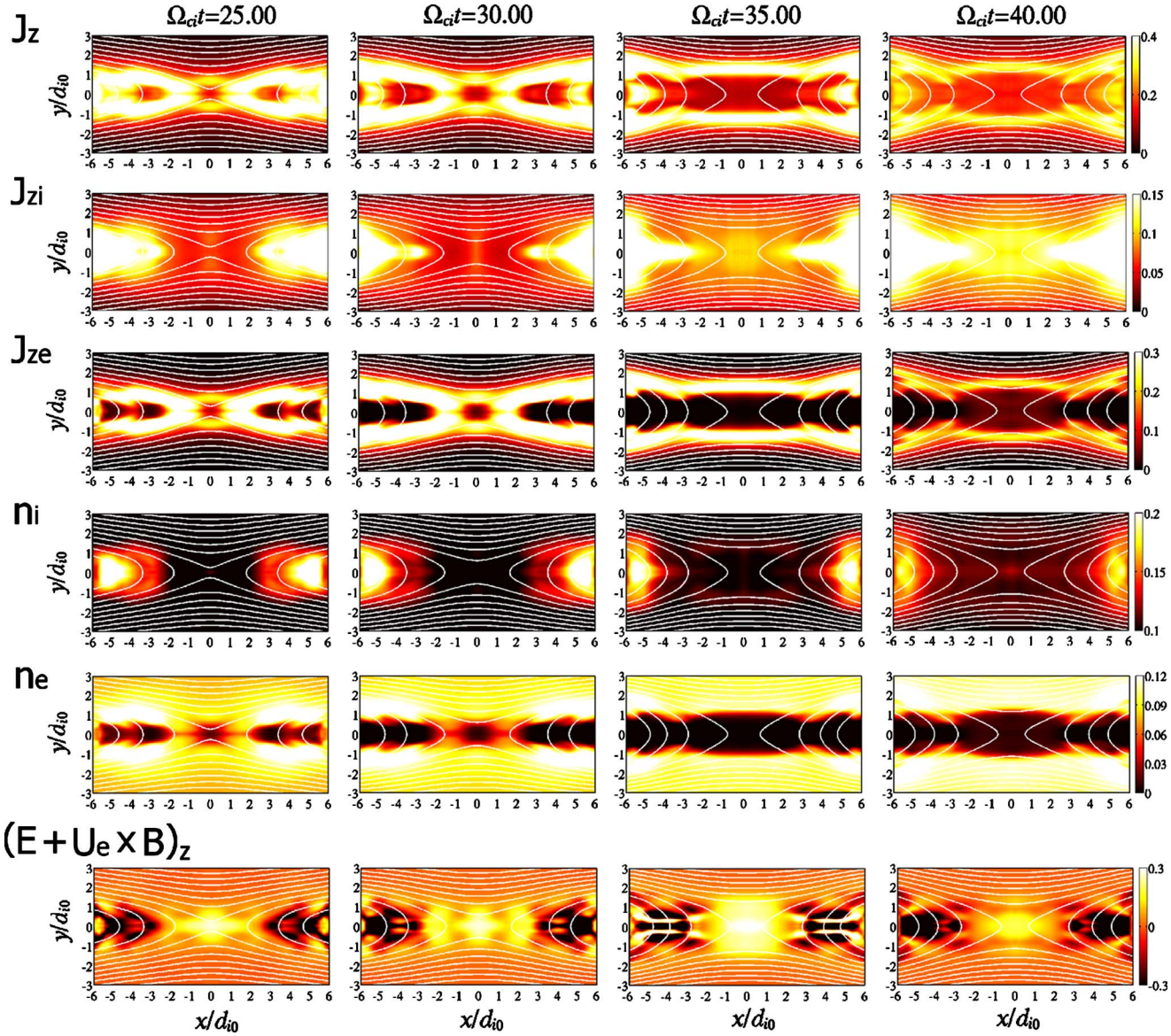

FIG. 3. (Color online) Spatial profiles of out-of-plane total current density J_z, ion current density J_{zi}, electron current density J_{ze}, ion number density n_i, electron number density n_e, and nonideal electric field for electrons $(\vec{E}+\vec{U}_e\times\vec{B})_z$ at different times. The current and number densities are normalized by $qn_0(V_{di0}-V_{de0})$ and n_0, respectively. The electric field is normalized by B_0V_{a0}.

reconnection rate of $E_z\sim 0.3B_0V_{a0}$. It should be noted that we use the normalization $B_0V_{a0}=(q_ic\Omega_{ci0}^2)/(m_i\omega_{pi0})$ where Ω_{ci0} and ω_{pi0} are defined at $y=\pm\infty$ and $y=0$, respectively, in common with the GEM reconnection challenge,[1] in which the maximum reconnection rate is $E_z\sim 0.25B_0V_{a0}$. If we use local Ω_{ci} and ω_{pi} for normalization, the maximum reconnection rate becomes $E_z\sim 0.1$. There exists the secondary peak of the reconnection rate at $\Omega_{ci0}t\sim 33$. However, generation of secondary magnetic islands[5] is not seen in the present simulation. After the secondary peak, the reconnection rate at the final state ($\Omega_{ci0}t\sim 40$) becomes $E_z\sim 0.2B_0V_{a0}$.

We first analyze the structures of current layers. Figure 3 shows spatial profiles of out-of-plane total current density J_z, ion current density J_{zi}, electron current density J_{ze}, ion number density n_i, electron number density n_e, and out-of-plane nonideal electric field for electrons $(\vec{E}+\vec{U}_e\times\vec{B})_z$ at different times, where $\vec{U}_e\equiv\vec{J}_e/(q_en_e)$ represents the electron bulk velocity. The current and number densities are normalized by $qn_0(V_{di0}-V_{de0})$ and n_0, respectively. The electric field is normalized by B_0V_{a0}.

It is shown in Fig. 3 that the out-of-plane current layer near the X-point is contributed by electrons, suggesting that ion and electron scales are clearly separated. The structure of the total current layer at $\Omega_{ci0}t=25$ is similar to that at $\Omega_{ci0}t=30$. At $\Omega_{ci0}t=25$, the strong ion current layer exists for $|x|>3d_{i0}$. The electron current layer has a double-peak structure for $|x|<d_{i0}$. At $\Omega_{ci0}t=30$, the electron-dominated current layer is elongated in the outflow direction, and the strong ion current layer exists for $|x|>5d_{i0}$. The double-peak electron current layer extends slightly in both inflow and outflow directions.

In the present Vlasov simulation, it is clearly shown that both ion and electron number densities decrease near the X-point, but on different spatial scales. The ion number den-

sity decreases for $|x|<3d_{i0}$, and the electron number density decreases in a narrower region ($|x|<d_{i0}$ and $|y|<0.5d_{i0}$). The spatial structures of the ion and electron number densities are correlated with their current-density structures. Thus, the spatial structure of the out-of-plane electron bulk velocity (not shown) becomes similar to that obtained in the previous PIC simulations. It is noted that we use the initial ion inertial length d_{i0} for normalization of spatial length. As shown in Fig. 3, the electron number density near the X-point changes drastically, and a "local" electron inertial length d_e becomes comparable to the initial ion inertial length.

In the time period $\Omega_{ci0}t=35-40$, the structure of the total current layer becomes different from that in the time period $\Omega_{ci0}t=25-30$. Although the structure of the ion current layer looks similar in both time periods, the structure of the electron current layer is very different. The double-peak electron current layer extends in both inflow and outflow directions. The low-electron-density region exists for $|y|<d_{i0}$ in the inflow direction and is elongated in the outflow direction. The second peak of the reconnection rate seen in Fig. 2 might correspond to the transition.

The structures of diffusion regions are sometimes identified by the out-of-plane component of the nonideal electric field, i.e., $(\vec{E}+\vec{U}_s\times\vec{B})_z$. The bottom panels of Fig. 3 show spatial profiles of the out-of-plane nonideal electric field for electrons at different times.

It is confirmed that the electron nonideal electric field has multiple structures (e.g., Refs. 6 and 7). There exists a positive nonideal electric field around the X-point. A negative nonideal electric field lays outside the positive region. The positive region has two structures. In the time period $\Omega_{ci0}t=25-30$, a thicker inner region exists for $|x|<0.5d_{i0}$ and $|y|<d_{i0}$, and a thinner outer region exists for $|x|<2d_{i0}$ and $|y|<0.5d_{i0}$. In the time period $\Omega_{ci0}t=35-40$, the inner positive region becomes wider in both inflow and outflow directions as the electron current layer. The negative region exists for $3d_{i0}<|x|<6d_{i0}$ and $|y|<d_{i0}$ for all period $\Omega_{ci0}t=25-40$. However, its structure is more complicated than the structure of the electron nonideal electric field seen in the previous PIC simulations.

Figure 4 shows the slices of electron number density, out-of-plane electron current density, and electron nonideal electric field at the center of the current sheet ($y=0$). The electron number density at the X-point is obtained as $n_e\sim0.005n_0$, which corresponds to the electron inertial length of $d_e\sim2.5d_{i0}$. At $\Omega_{ci0}t=30$, the electron number density near the X-point varies from $0.005n_0$ to $0.05n_0$. Thus, the average electron inertial length is $d_e\sim1.2d_{i0}$.

From Fig. 4, we found that the essential structures of the electron diffusion region on the x-axis are similar at $\Omega_{ci0}t=30$ and 40, although its spatial profiles (Fig. 3) look different. The full width of the inner region with positive nonideal electric field corresponds to twice the electron inertial length at the X-point. In the outer region with negative nonideal electric field, a typical electron number density is obtained as $n_e\sim0.0005n_0$, which corresponds to the electron inertial length $d_e\sim8d_{i0}$. The full width of the outer region is

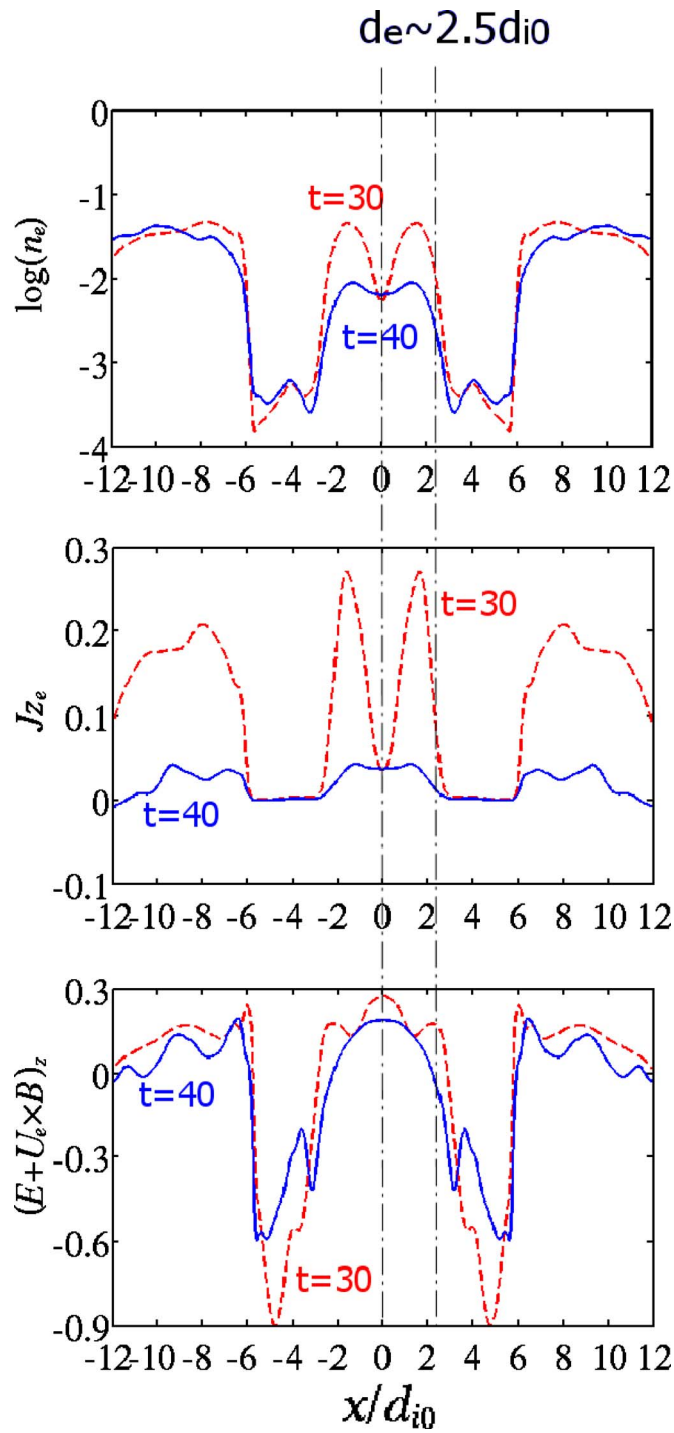

FIG. 4. (Color online) Spatial profiles of electron number density n_e, out-of-plane electron current density J_{ze}, and electron nonideal electric field $(\vec{E}+\vec{U}_e\times\vec{B})_z$ at $\Omega_{ci0}t=30$ and 40 sliced at $y=0$. The number and current densities are normalized by n_0 and $qn_0(V_{di0}-V_{de0})$, respectively. The electric field is normalized by B_0V_{a0}.

slightly shorter than twice the electron inertial length in the outer region. The ion number density in the electron diffusion region is $n_i\sim0.1n_0$ (not shown). Thus, the electron inertial length becomes longer than the ion inertial length in the outer region.

In Fig. 3, we found that the electron diffusion region extends in the inflow direction as well as the outflow direc-

tion in the time period $\Omega_{ci0}t=35-40$. However, this result is not surprising because the electron number density decreases and the electron inertial length becomes longer in this period.

IV. SUMMARY

In the present Vlasov simulation, it is confirmed that the full thickness of the inner electron diffusion region becomes equivalent to the local electron inertial length. The electron number density in the electron diffusion region decreases drastically ($<10^{-2}n_0$) during magnetic reconnection. Note that one needs more than 1000 particles per cell to treat such a small number density with the PIC method. However, PIC simulations of magnetic reconnection typically used 100 particles per cell, in which numerical thermal fluctuations would be enhanced. A low-noise Vlasov simulation allows us to resolve detailed structures of the electron diffusion region. It is expected that different structures would be obtained in asymmetric reconnection, which is left as a future work.

It should be noted that the spatial length of the simulation domain is not so long in the present Vlasov simulation. In the previous PIC simulations, the spatial scale of the electron diffusion region in the outflow direction is much longer than that in the present Vlasov simulation because the spatial length of the simulation domain is also much longer (e.g., Refs. 4–7). During the extension of the electron diffusion region, generation of secondary magnetic islands is also reported.[5,6] The spatial length of the simulation domain would be extended in a future study. However, this requires numerous computational resources.

ACKNOWLEDGMENTS

This work was supported by Grant-in-Aid for Young Scientists (B) (Grant No. 21740352) and in part by Grant-in-Aid for Creative Scientific Research (Grant No. 17GS0208) from MEXT of Japan. The computer simulations were performed on the Fujitsu FX1 and HX600 supercomputer systems at Information Technology Center (ITC) in Nagoya University. The computational resource was provided by Solar-Terrestrial Environment Laboratory (STEL) in Nagoya University as a collaborative computational research project.

[1] J. Birn, J. F. Drake, M. A. Shay, B. N. Rogers, R. E. Denton, M. Hesse, M. Kuznetsova, Z. W. Ma, A. Bhattacharjee, A. Otto, and P. L. Pritchett, J. Geophys. Res. **106**, 3715, doi:10.1029/1999JA900449 (2001).
[2] B. N. Rogers, R. E. Denton, J. F. Drake, and M. A. Shay, Phys. Rev. Lett. **87**, 195004 (2001).
[3] M. A. Shay, J. F. Drake, B. N. Rogers, and R. E. Denton, J. Geophys. Res. **106**, 3759, doi:10.1029/1999JA001007 (2001).
[4] K. Fujimoto, Phys. Plasmas **13**, 072904 (2006).
[5] W. Daughton, J. Scudder, and H. Karimabadi, Phys. Plasmas **13**, 072101 (2006).
[6] H. Karimabadi, W. Daughton, and J. Scudder, Geophys. Res. Lett. **34**, L13104, doi:10.1029/2007GL030306 (2007).
[7] M. A. Shay, J. F. Drake, and M. Swisdak, Phys. Rev. Lett. **99**, 155002 (2007).
[8] J. Scudder and W. Daughton, J. Geophys. Res. **113**, A06222, doi:10.1029/2008JA013035 (2008).
[9] K. Fujimoto and R. D. Sydora, Phys. Plasmas **16**, 112309 (2009).
[10] T. D. Phan, J. F. Drake, M. A. Shay, F. S. Mozer, and J. P. Eastwood, Phys. Rev. Lett. **99**, 255002 (2007).
[11] L.-J. Chen, N. Bessho, B. Lefebvre, H. Vaith, A. Fazakerley, A. Bhattacharjee, P. A. Puhl-Quinn, A. Runov, Y. Khotyaintsev, A. Vaivads, E. Georgescu, and R. Torbert, J. Geophys. Res. **113**, A12213, doi:10.1029/2008JA013385 (2008).
[12] H. Schmitz and R. Grauer, Comput. Phys. Commun. **175**, 86 (2006).
[13] T. Umeda, K. Togano, and T. Ogino, Comput. Phys. Commun. **180**, 365 (2009).
[14] K. S. Yee, IEEE Trans. Antennas Propag. **AP-14**, 302 (1966).
[15] C. Z. Cheng and G. Knorr, J. Comput. Phys. **22**, 330 (1976).
[16] A. Ghizzo, F. Huot, and P. Bertrand, J. Comput. Phys. **186**, 47 (2003).
[17] H. Schmitz and R. Grauer, Phys. Plasmas **13**, 092309 (2006).
[18] T. Umeda, Earth, Planets Space **60**, 773 (2008).
[19] E. G. Harris, Nuovo Cimento **23**, 115 (1962).
[20] E. L. Lindman, J. Comput. Phys. **18**, 66 (1975).
[21] G. Mur, IEEE Trans. Electromagn. Compat. **EMC-23**, 377 (1981).
[22] J. P. Berenger, J. Comput. Phys. **114**, 185 (1994).
[23] T. Umeda, Y. Omura, and H. Matsumoto, Comput. Phys. Commun. **137**, 286 (2001).